# Beam Breakup Simulations for the Scorpius Flash-Radiography Accelerator

Ekdahl, Carl August Jr.
Kurennoy, Sergey S.
Mccrady, Rodney Craig
Dale, Gregory E.



**To be published in:** IEEE Transactions on Plasma Science

**DOI to publisher's version:** 10.1109/TPS.2022.3147170





# Beam Breakup Simulations for the Scorpius Flash-Radiography Accelerator

Carl Ekdahl, Sergey Kurennoy, Rodney McCrady, and Gregory Dale

***Abstract*— Beam breakup (BBU) in linear induction accelerators (LIAs) used for flash radiography is problematic because the high-frequency beam motion can blur the source spot, thereby degrading resolution. Amplification of BBU depends directly on details of cell design and is suppressed in operation by the solenoidal magnetic field focusing on the electron beam. Therefore, much effort has gone into design of the cells and magnetic focusing for the new Scorpius radiography LIA. In this article, we use computer simulations to demonstrate that BBU in Scorpius should be no more than in present radiography LIAs at the Los Alamos National Laboratory.**

***Index Terms*— Beam breakup (BBU), electron beam accelerators, electron beam stability, transverse impedance.**

## I. Introduction

THE most dangerous instability for electron linear induction accelerators (LIAs) is the beam breakup (BBU) instability [1]–[3]. For flash-radiography LIAs, it is particularly troublesome, because even if it is not strong enough to destroy the beam, the high-frequency BBU motion can blur the source spot, which is time-integrated over the pulsewidth.

In an LIA, the beam excites cavity RF. The transverse magnetic field modes deflect the beam, causing RF oscillation of the beam centroid. The beam pipe is a waveguide beyond cutoff for the lowest resonant frequencies, so cavities can only communicate via beam oscillations and not by electromagnetic waves. The resulting instability is called cumulative BBU.

In an LIA with a fast rise time current pulse, BBU oscillations excited by the sharp beam head grow to a peak and then decay [2], [4]. The instability is convective, and the peak moves back in the pulse as it propagates. If the amplitude is large enough, the tail end of the beam spills onto the beam pipe, and the current pulsewidth shrinks as it propagates through the LIA, hence the name of the observed effect.

For a large enough number of accelerating cells, the maximum BBU amplitude asymptotes to

$$\xi(z) = \xi_0\left[\gamma_0/\gamma\,(z)\right]^{1/2}\exp(\Gamma_m) \tag{1}$$

This work was supported by the U.S. Department of Energy through the Los Alamos National Laboratory. Los Alamos National Laboratory is operated by Triad National Security, LLC, for the National Nuclear Security Administration of U.S. Department of Energy under Contract 89233218CNA000001.

The authors are with the Los Alamos National Laboratory, Los Alamos, NM 87545 USA (e-mail: cekdahl@lanl.gov).

where subscript zero denotes initial conditions and $\gamma$ is the relativistic mass factor. The maximum growth exponent in this equation is

$$\Gamma_m(z) = \frac{I_{kA}N_g Z_{\perp\Omega/m}}{3\times 10^4}\left\langle\frac{1}{B_{kG}}\right\rangle \tag{2}$$

where $I_{kA}$ is the beam current in kA, $N_g$ is the number of gaps, $Z_{\perp\Omega/m}$ is the transverse impedance in $\Omega$/m, $B_{kG}$ is the guide field in kG, and $\langle\rangle$ indicates averaging over $z$ [3], [4]. This theoretical growth of BBU in high-current LIAs has been experimentally confirmed [5]–[8] and has been used to design magnetic transport that suppresses BBU amplification to acceptable levels [9]–[12].

For a high-current LIA with a given number of cells needed to achieve the required endpoint energy, (2) shows how BBU growth depends on the transverse impedance $Z_\perp$ of the accelerating gaps and associated cavities. The impedance scaling with physical dimensions is roughly [13]

$$Z_\perp = Z_0\frac{w}{b^2}\eta \tag{3}$$

where $Z_0 = 120\pi\,\Omega$ is the impedance of free space, $w$ is the width of the accelerating gap, $b$ is the radius of the beam pipe, and $\eta$ is a form factor associated with cavity details. Since the gap width is limited by the required accelerating potential and the pipe size is limited by a multitude of engineering factors, a significant effort has been devoted to reducing the form factor in order to minimize the transverse impedance and BBU amplification.

Equation (2) also shows how the BBU amplitude is suppressed by the solenoidal magnetic focusing used to transport the beam. Increasing the number of cells with a given impedance must be offset by an increase in field strength. For an LIA with given impedance, operational control of the instability critically depends on effective tuning of available solenoidal field strength, which may be limited by engineering constraints.

The dual-axis radiographic hydrodynamic testing (DARHT) facility at the Los Alamos National Laboratory (LANL) uses two electron LIAs to produce the source spots for flash radiography of large explosively driven experiments by focusing the electron beam onto a heavy metal target [14]–[17], and a new multipulse LIA, Scorpius, is under development for this purpose [18]. Since Scorpius will have 50% more cells than previous radiography LIAs, it is important to assess its vulnerability to BBU and whether the design magnetic fields will be sufficient for suppression.

TABLE I
DARHT-I PARAMETERS

| Parameter | Symbol | Units | Value |
|---|---|---|---|
| **Beam:** | | | |
| **Injected Kinetic Energy** | $KE_0$ | MeV | 3.71 |
| **Final Kinetic Energy** | $KE_f$ | MeV | 19.6 |
| **Current** | $I_b$ | kA | 1.75 |
| **Accelerator:** | | | |
| **Number of Cells** | $N$ | | 64 |
| **Length** | $L$ | cm | 3430 |
| **Pitch** | $\ell$ | cm | 43.2 |
| **Tuned Guide Field** | $B_z$ | kG | Fig. 1 |

In this article, we use numerical simulations based on recent measurements of transverse impedance to investigate the expected BBU in Scorpius. We describe these BBU simulations in Section II.

## II. SIMULATIONS

Our LAMDA beam dynamics code is used for these simulations [19]. LAMDA stands for Linear Accelerator Model for DARHT, and the LAMDA BBU algorithm is briefly described in Appendix A. All simulations are based on recent transverse impedance measurements.

### A. DARHT-I

The DARHT-I LIA provides the electron beam for single-pulse flash radiography. A fast rise time current pulse with 60-ns flat-top created by a 3.71-MV diode is accelerated to 19.6 MeV by 64 induction cells and focused onto a thin heavy metal target to create the source spot for point projection radiographs. Solenoidal magnetic fields are used to transport the beam, with each cell containing a solenoid as well as an inductively isolated accelerating gap. Parameters of DARHT-I used in our simulations are listed in Table I. The magnetic field on axis for a tune of the DARHT-I LIA used for many radiographs over the past decade is shown in Fig. 1, along with the beam size calculated by our XTR envelope code [20]. The XTR and LAMDA models for the DARHT magnetic field are based on experimental measurements [21].

The voltage pulse is applied to the accelerating gap by a pair of drive rods in the horizontal plane, which breaks the cell-cavity symmetry, that is, the $TM_{1n0}$ electromagnetic fields responsible for BBU couple to the rods differently depending on the orientation of the plane of the beam BBU oscillation. This asymmetry in coupling results in a different transverse impedance for oscillations in the $x$-plane versus oscillations in the $y$-plane. Moreover, as the beam transports through the axial magnetic field, the Larmor rotation of the plane of oscillation causes the beam to couple to the cells differently depending on its phase. This natural "stagger tuning" helps suppress BBU because the net result is that it is amplified as if by a single impedance that is the average of the two polarizations, hence less than either [22]. However, the simulations reported in this article used the different transverse impedances for vertical versus horizontal polarizations.

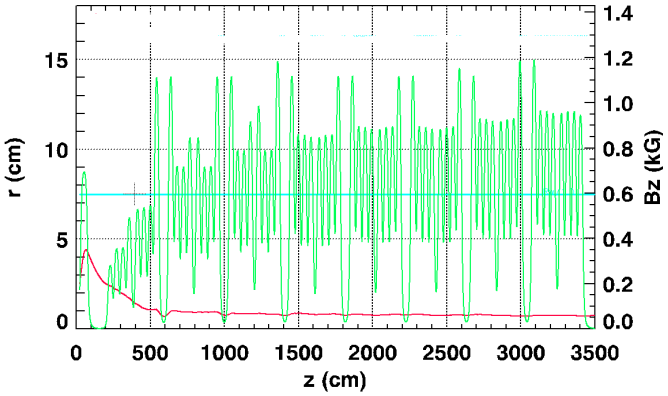


Fig. 1. Beam envelope in DARHT-I as calculated by the XTR envelope code. The distance $z$ is measured from the cathode surface. Red curve: beam envelope (left scale). Green curve: axial magnetic field on axis (right scale). Cyan line: beam pipe wall at a radius of 7.41 cm. In this plot, $z = 0$ is defined as the emission surface of the cathode.

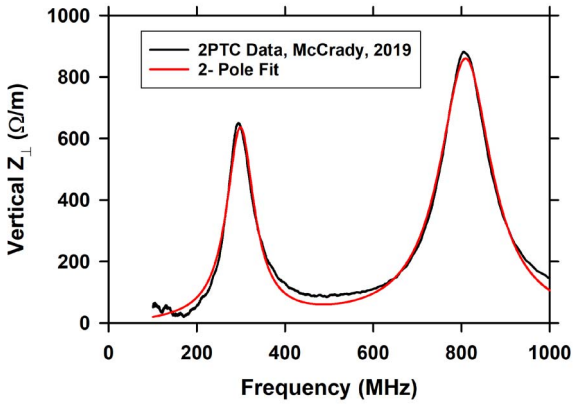


Fig. 2. Measurement of the coupling impedance for beam oscillations in the vertical plane [23]. Black curve: experimental data. Red curve: two-pole wakefield impedance fit to data.

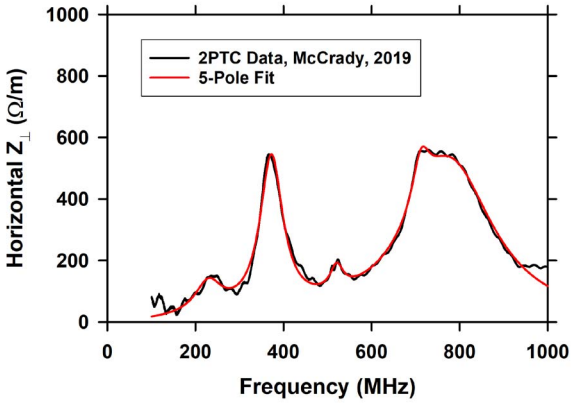


Fig. 3. Measurement of the coupling impedance for beam oscillations in the horizontal plane [23]. Black curve: experimental data. Red curve: five-pole wakefield impedance fit to data.

The vertical and the horizontal coupling have recently been remeasured [23], and Figs. 2 and 3 show the LAMDA wakefield impedance model fitted to these measurements. Our LAMDA simulations of BBU are based on these modern

TABLE II

DARHT-I VERTICAL TRANSVERSE IMPEDANCE MODEL

| Frequency | Amplitude | Quality |
|---|---|---|
| $f_n$ | $Z_{\perp n}$ | $Q_n$ |
| MHz | Ω/m | |
| 298.69 | 623.79 | 3.973 |
| 809.32 | 857.93 | 5.651 |

TABLE III

DARHT-I HORIZONTAL TRANSVERSE IMPEDANCE MODEL

| Frequency | Amplitude | Quality |
|---|---|---|
| $f_n$ | $Z_{\perp n}$ | $Q_n$ |
| MHz | Ω/m | |
| 229.38 | 103.61 | 3.055 |
| 372.35 | 501.76 | 5.878 |
| 520.66 | 79.45 | 14.285 |
| 712.09 | 164.32 | 14.575 |
| 777.78 | 513.92 | 3.241 |

measurements. The parameters of the fits are listed in Tables II and III.

BBU can be initially excited in several different ways. Rapidly increasing energy on the pulse leading edge can give rise to high-frequency corkscrew motion that can be a source of excitation [24]. A fast current rise time of an initially offset beam can also excite BBU. Even if the rise time is slow, BBU can grow out of other sources of weak RF or noise, as in DARHT-II [5]. The design of DARHT-I is such that the gap voltage pulse entirely overlaps the shorter beam current pulse, thereby circumventing large corkscrew on the beam head. Moreover, the rise time is too slow to effectively excite BBU, and the observed amplification is insignificant with the nominal magnetic tune shown in Fig. 1. In fact, in order to make meaningful experimental measurements, the magnetic field had to be significantly reduced [7], [8].

Therefore, in order to compare simulations, we resort to initial excitation with single frequency sine waves at the frequency of maximum growth. This resonant excitation method decouples the result from the frequency content of the current pulse, and the amplification is a property of the accelerator alone, so it is most useful for comparing accelerator structures or magnetic tunes [10], [11]. Moreover, for consistent comparisons, all simulations were started 5-cm upstream of the first gap and ended 5-cm downstream of the last gap.

For these simulations of DARHT-I, the constant-current beam was excited by an 800-MHz sine wave, corresponding to the peak of the average impedance. The resulting amplification is shown in Fig. 4 where it is seen that this worst case of excitation at the peak resonant frequency results in amplification of less than 20, as if coupled by an impedance equal to an average of horizontal and vertical due to a natural "stagger-tuning" effect [22].

### *B. Scorpius*

Scorpius is a new multipulse LIA being developed for flash radiography [18]. Unlike DARHT-II, Scorpius will generate multiple beam pulses in its 2-MeV, 1.45-kA injector, and then

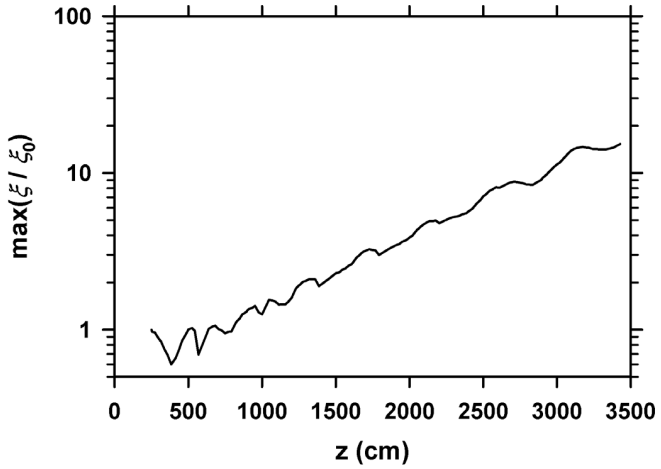


Fig. 4. LAMDA simulation of BBU amplification for asymmetric vertical and horizontal impedances shown in Figs. 2 and 3. In this plot, $z = 0$ is defined as the emission surface of the cathode.

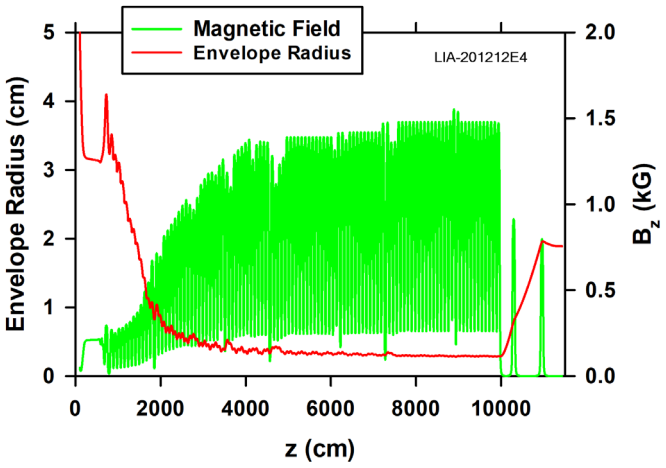


Fig. 5. Beam envelope in Scorpius as calculated by the XTR envelope code, illustrating magnetic transport from the diode to final focus. Red curve: beam envelope radius (left scale). Green curve: axial magnetic field on axis of focusing solenoids (right scale). In this plot, the beam-pipe wall at a radius of 7.41 cm is off scale. In this plot, $z = 0$ is defined as the emission surface of the cathode.

accelerate them to 22.4 MeV with 102 cells with 200-keV gaps. Accelerating gap voltages for the Scorpius LIA will be produced with solid-state pulsed power (SSPP) [25]–[27]. As in DARHT-I, beam transport will be accomplished with solenoidal focusing. By comparison, Scorpius will be more than twice as long as DARHT-I and will have peak magnetic fields about 50% stronger. Fig. 5 shows a nominal magnetic tune for Scorpius that has negligible emittance growth as evidence of a stable envelope [28]. The XTR and LAMDA models for the Scorpius magnetic field are based on finite-element simulations of the design, including all magnetic materials such as Metglas and ferrite [21]. The Scorpius beam parameters are listed in Table IV.

A significant effort was invested in the design of the Scorpius accelerating cell in order to minimize the transverse impedance. First, the DARHT-I gap and insulator design was retained because it had been shown to reduce the impedance [29]. Moreover, this gap was reliable at twice the

TABLE IV

SCORPIUS PARAMETERS

| Parameter | Symbol | Units | Value |
|---|---|---|---|
| **Beam:** | | | |
| **Injected Kinetic Energy** | $KE_0$ | MeV | 2 |
| **Final Kinetic Energy** | $KE_f$ | MeV | 22.4 |
| **Current** | $I_b$ | kA | 1.45 |
| **Accelerator:** | | | |
| **Number of Cells** | $N$ | | 102 |
| **Length*** | $L$ | cm | 9100 |
| **Pitch** | $\ell$ | cm | 86.7 |
| **First Gap** | $z_{g1}$ | cm | 882.8 |
| **Tuned Guide Field** | $B_z$ | kG | Fig. 5 |

*First to last gap

TABLE V

SCORPIUS TRANSVERSE IMPEDANCE MODEL

| Frequency | Amplitude | Quality |
|---|---|---|
| $f_n$ | $Z_{\perp n}$ | $Q_n$ |
| MHz | Ω/m | |
| 219.82 | 192.82 | 22.744 |
| 267.32 | 192.05 | 1.999 |
| 375.97 | 79.30 | 2.673 |
| 630.33 | 251.18 | 3.256 |
| 668.61 | 273.51 | 18.696 |
| 735.54 | 337.87 | 9.216 |
| 787.92 | 203.57 | 15.882 |
| 837.71 | 193.82 | 11.873 |
| 914.60 | 130.42 | 20.727 |
| 1020.22 | 81.78 | 24.541 |
| 1160.47 | 195.95 | 4.225 |

required voltage withstand in single-pulse testing [29], and it proved to be reliable in multiple-pulse tests for Scorpius. Moreover, a substantial effort was devoted to further optimizing the cavity design through experiments with mock-up cells that were guided by extensive computer simulations using CST Studio electromagnetic codes [30].

An efficient method of calculating impedances in cavities with dispersive ferrites using CST has been developed, and. the calculation results agree well with measurements for prototype cavities [31]. The CST modeling was used for extensive evaluation of damping ferrite materials and geometries, as well as the geometry of the cavity, in order to reduce the impedance. The resulting impedance measured on a prototype accelerator cell (PAC) is shown in Fig. 6. The LAMDA wakefield impedance model is also shown (Appendix), which required including 11 resonances (poles) to fit to the measured data. Table V lists the fitted model parameters.

The growth of BBU in Scorpius simulations is shown in Fig. 7. The constant-current beam was excited at the 668-MHz resonant frequency of the dominant mode shown in Fig. 6. BBU growth in DARHT-I excited at 800 MHz is also displayed for comparison, near its maximum coupling impedance.

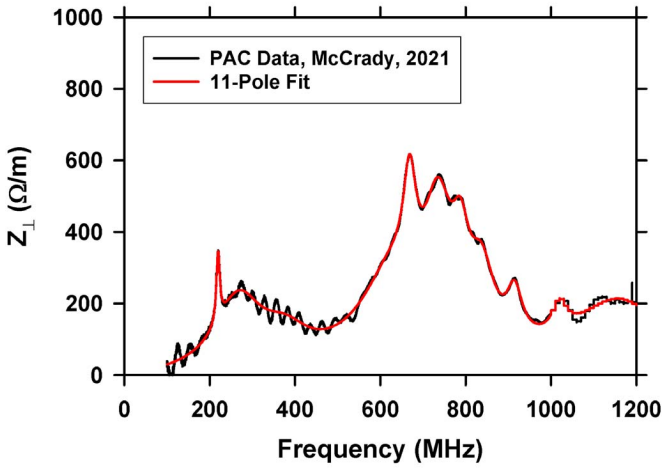


Fig. 6. Measurement of the Scorpius PAC coupling impedance. Black curve: experimental data [31]. Red curve: 11-pole wakefield impedance fit to data.

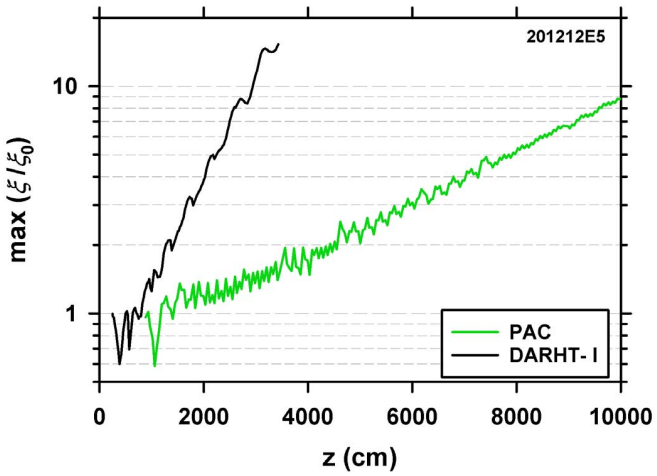


Fig. 7. Comparison of BBU in Scorpius with DARHT-I. Black curve: DARHT-I BBU amplification using wakefield impedance model fit to asymmetric impedance measurements. Green curve: Scorpius BBU amplification using the wakefield impedance model fit to the measured impedance of PAC. In this plot, $z = 0$ is defined as the emission surface of the cathode.

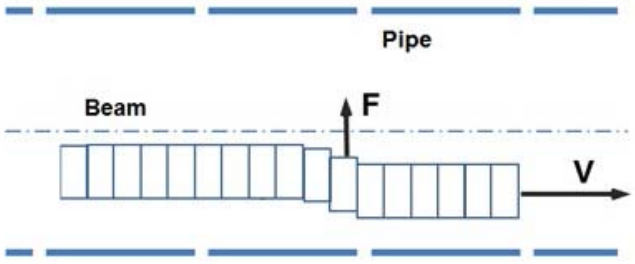


Fig. 8. Articulated beam model used by LAMDA to calculate the motion of the beam centroid.

The oscillations of the Scorpius growth curve, especially evident between 46 and 73 m in Fig. 7, correlate with weak betatron oscillations on the beam envelope (Fig. 5), which are evidence of a slight mismatch that disappears as the beam is more tightly focused at the end of the LIA.

Both DARHT and Scorpius growth curves begin at the first cell, which in Scorpius is much further from the cathode located at $z = 0$. Thus, even though longer and having

more cells, growth of resonantly excited BBU is less in Scorpius than in DARHT-I, as simulated by LAMDA. Since the maximum transverse impedances are about the same, this is due to the stronger magnetic fields used for the Scorpius tune shown in Fig. 5 compared with that for DARHT-I shown in Fig. 1. Since the Scorpius solenoids are capable of producing peak fields 30% greater than those shown in Fig. 5, even this can be improved.

## III. Discussion and Conclusion

In this article, we have investigated the amplification of the BBU instability predicted for the new Scorpius LIA based on recent measurements of the transverse impedance of a PAC. The results of BBU simulations show less growth in Scorpius than in DARHT-I when the instability is resonantly excited in a manner that decouples from the current-pulse waveform, that is, the simulations were a direct comparison of accelerator structures and magnetic transport tune, independent of the current pulse. Since current-pulse excited BBU does not appear to noticeably enlarge the radiographic source spot on DARHT-I, these results indicate that the Scorpius spot will also be unaffected.

## Appendix A

We use the LAMDA beam dynamics code to understand BBU in our LIAs. LAMDA is discretized in both space and time; for given accelerator properties and an arbitrary input pulse, $I_b(t), KE(t)$, the results are the centroid position in space and time, $x(z,t), y(z,t)$.

### A. Time Resolution

LAMDA simulates beam motion due to external forces by subdividing the beam into many disks, as shown in Fig. 8, and calculating the motion of each disk from the force on its center. For a relativistic beam, it is assumed that there is no interaction between the beam disks. The full set of differential equations to be solved for the beam centroid motion are the equations for the spatial motion of each beam disk along the accelerator and the equations for the temporal variation of the voltage and BBU forces at the gaps.

### B. BBU Algorithm

The interaction of the disk with the dipole $TM_{1n0}$ fields at the gap is calculated using the narrow gap approximation, that is, the beam position is assumed to be invariant as the beam crosses the gap, but a transverse impulse is applied. A disk that arrives at a gap at time $t$ measured back from the head of the beam receives a transverse impulse given by

$$\frac{\Delta p_x(t)}{mc} = \int_0^t \boldsymbol{\mathcal{Z}}_x(t-\tau)\,\imath(\tau)\xi(\tau)cd\tau \equiv \int_0^t \boldsymbol{\mathcal{Z}}_x(t-\tau)\,f(\tau)cd\tau \tag{4}$$

and similarly for $\Delta p_y(t)$. Here, $\xi(t)$ is the disk displacement from the magnetic centerline in the $x$-direction, and $\imath(t) = I_b(t)/I_0$, where $I_0 = 4\pi m_e c/\mu_0 e = 17.05$ kA. Also, $\boldsymbol{\mathcal{Z}}_x(t)$ is the wake function for the cavity. Since the convolution integral is the Fourier transform of the product of the transforms of the integrand, this equation can be solved by using the inverse transform of that product, that is,

$$\frac{\Delta p_x(t)}{mc} = \int_{-\infty}^{\infty} Z(\omega)F(\omega)e^{-i\omega t}\,d\omega \tag{5}$$

where $F(\omega)$ is the Fourier transform of $f(t)$ and the impedance $Z(\omega)$ is the transform of the wake function $\boldsymbol{\mathcal{Z}}(t)$. The wake function is real, so the real part of $Z(\omega)$ is symmetric, and $Z_\perp(\omega) = -iZ(\omega)$ to give a coupling impedance with antisymmetric real part that vanishes for zero frequency, as it must [4].

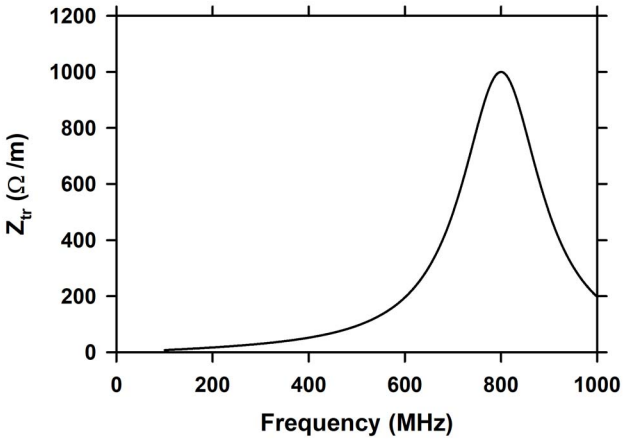


Fig. 9. Real part of transverse impedance that is responsible for the BBU instability. The LAMDA wakefield model used example parameters from Table I.

### C. Impedance Model

The transverse wakefield impedance used in LAMDA is [32]–[34]

$$Z_\perp = \sum_n Z_{\perp n}\ \frac{1}{1+2i\,Q_n(\omega/\omega_n - 1)} - \frac{1}{1+2i\,Q_n(\omega/\omega_n + 1)}\ . \tag{6}$$

Because theoretical expressions for transverse impedance vary in the phase relation between real and complex components depending on author, it is useful to remember that the component responsible for BBU coupling is real, satisfies $Z_\perp(-\omega) = -Z_\perp(\omega)$ (antisymmetric), and vanishes at the origin [4]. LAMDA has the capability for using different impedances for vertical and horizontal polarizations to accommodate the known asymmetries of the DARHT cells. At present, the code can also accommodate up to 12 different resonant frequencies.

### D. Beam Breakup (BBU) Instability

LAMDA simulations of BBU growth agree with the well-known analytic result for asymptotic growth rate in a uniform, axial magnetic field. For example, consider an accelerator consisting of 100 cells, each with peak transverse impedance of 10 Ω/cm at 800 MHz (Fig. 9). For this simulation, the BBU was excited by a fast rising 2-kA pulse (Fig. 10) injected with

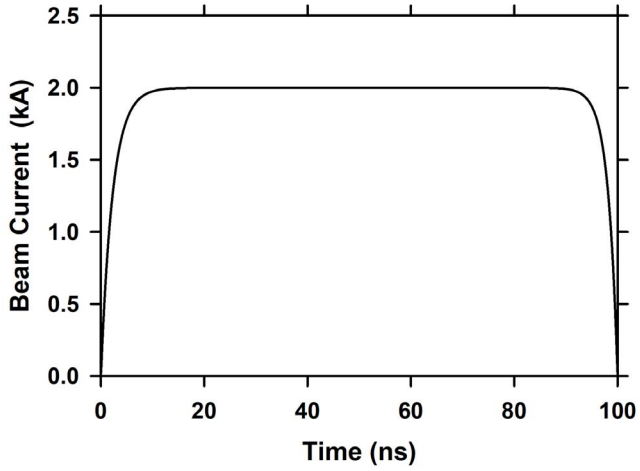


Fig. 10. Current pulse used for example simulation of BBU growth. For the example simulation, this pulse was initiated with an offset of 1 mm in the $x$-direction.

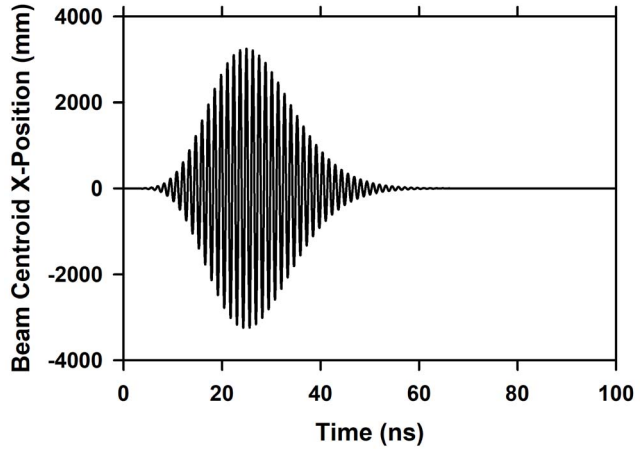


Fig. 11. Beam centroid motion resulting from BBU calculated by LAMDA for the example. The beam position in the horizontal plane at the LIA exit ($z = 8000$ cm) is shown.

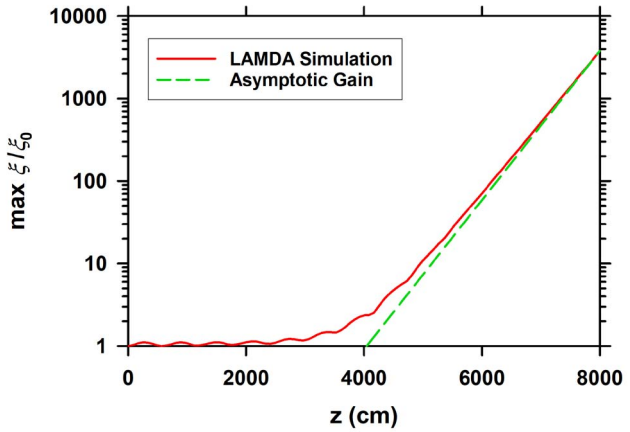


Fig. 12. BBU growth in the example LIA. Red curve: growth simulated by LAMDA. Green dashed line: asymptotic growth from (1) using example parameters from Table VI with a delayed start.

a 1-mm offset. The rest of the parameters of the simulation are shown in Table VI. The $x$-component of the resulting RF motion at the exit of the LIA is shown in Fig. 11. Fig. 12 shows a plot of the maximum amplitude of the displacement (over the beam pulselength) as a function of propagation distance. From analytic theory, this displacement should converge asymptotically to an exponential growth according to (1), which it does after a delay, as evident in Fig. 12.

TABLE VI
BBU EXAMPLE PARAMETERS

| Parameter | Symbol | Units | Value |
|---|---|---|---|
| **Beam:** | | | |
| **Kinetic Energy** | $KE$ | MeV | 10 |
| **Current** | $I_b$ | kA | 2 |
| **Pulse Risetime** | $\tau_r$ | ns | 5 |
| **Pulse Flattop** | $\tau_{flat}$ | ns | 60 |
| **Pulse Falltime** | $\tau_f$ | ns | 4 |
| **Initial Offset** | $x_0$ | mm | 1 |
| **Induction Cell:** | | | |
| **Resonant Frequency** | $f_0$ | MHz | 800 |
| **Peak Impedance** | $Z_\perp$ | Ω /cm | 10 |
| **Quality Factor** | $Q$ | | 4 |
| **Accelerator:** | | | |
| **Number of Cells** | $N$ | | 100 |
| **Length** | $L$ | cm | 8000 |
| **Pitch** | $\ell$ | cm | 80 |
| **Uniform Guide Field** | $B_z$ | kG | 0.4 |

In actuality, the BBU amplitude in this simple example grows enough that a significant portion of the pulse would be scraped off on the beam pipe long before the pulse transported to the exit. For example, according to Fig. 12, the beam oscillations would begin scraping on a 15-cm-diameter pipe at about ¾ of the distance to the exit, and the pulse would be severely eroded before reaching the accelerator exit.

## ACKNOWLEDGMENT

The authors are deeply indebted to their colleagues at Los Alamos and elsewhere for stimulating discussions on charged particle beam physics and many other topics.

## REFERENCES

[1] R. Helm, "Computer study of wave propagation, beam loading, and beam blowup in the SLAC accelerator," in *Proc. Linear Accel. Conf.*, Los Alamos, NM, USA, 1966, pp. 1–13.

[2] W. K. H. Panofsky and M. Bander, "Asymptotic theory of beam-breakup in linear accelerators," *Rev. Sci. Instrum.*, vol. 39, pp. 206–212, Dec. 1968.

[3] V. K. Neil, L. S. Hall, and R. K. Cooper, "Further theoretical studies of the beam breakup instability," *Particle Accel.*, vol. 9, no. 4, pp. 213–222, 1979.

[4] G. J. Caporaso and Y.-J. Chen, "Electron induction linacs," in *Induction Accelerators*, K. Takayama R. J. Briggs, Eds. New York, NY, USA: Springer, 2011, pp. 117–163.

[5] C. Ekdahl *et al.*, "Long-pulse beam stability experiments on the DARHT-II linear induction accelerator," *IEEE Trans. Plasma Sci.*, vol. 34, no. 2, pp. 460–466, Apr. 2006.

[6] C. Ekdahl *et al.*, "Beam dynamics in a long-pulse linear induction accelerator," *J. Korean Phys. Soc.*, vol. 59, no. 6, pp. 3448–3452, 2011.

[7] J. E. Coleman, C. A. Ekdahl, D. C. Moir, G. W. Sullivan, and M. T. Crawford, "Correcting the beam centroid motion in an induction accelerator and reducing the beam breakup instability," *Phys. Rev. ST Accel. Beams*, vol. 17, Sep. 2014, Art. no. 092802.

[8] J. E. Coleman *et al.*, "Increasing the intensity of an induction accelerator and reduction of the beam breakup instability," *Phys. Rev. ST Accel. Beams*, vol. 17, Mar. 2014, Art. no. 030101.

[9] C. Ekdahl *et al.*, "Suppressing beam-centroid motion in a long-pulse linear induction accelerator," *Phys. Rev. Special Topics-Accel. Beams*, vol. 14, no. 12, Dec. 2011, Art. no. 120401.

[10] C. Ekdahl, "Electron-beam dynamics for an advanced flash-radiography accelerator," *IEEE Trans. Plasma Sci.*, vol. 43, no. 12, pp. 4123–4129, Dec. 2015.

[11] C. Ekdahl, J. E. Coleman, and B. T. McCuistian, "Beam breakup in an advanced linear induction accelerator," *IEEE Trans. Plasma Sci.*, vol. 44, no. 7, pp. 1094–1102, Jul. 2016.

[12] C. Ekdahl, "Beam breakup simulations for a solid state powered linear induction accelerator," Los Alamos Nat. Lab., Los Alamos, NM, USA, Tech. Rep. LA-UR-20-22662, 2020.

[13] K. Takayama and R. J. Briggs, *Induction Accelerators*. New York, NY, USA: Springer, 2011.

[14] M. J. Bums *et al.*, "Status of the DARHT phase 2 long-pulse accelerator," in *Proc. PACS. Proc. Part. Accel. Conf.*, Chicago, IL, USA, 2001, pp. 1–5.

[15] C. Ekdahl, "Modern electron acccelerators for radiography," *IEEE Trans. Plasma Sci.*, vol. 30, no. 1, pp. 254–261, Feb. 2002.

[16] R. Briggs and G. Westenskow, "Historical perspectives," in *Induction Accelerators*. Berlin, Germany: Springer-Verlag, 2011, pp. 7–22.

[17] K. Peach and C. Ekdahl, "Particle radiography," *Rev. Acc. Sci. Tech.*, vol. 6, pp. 117–142, Oct. 2013.

[18] M. Crawford and J. Barraza, "Scorpius: The development of a new multi-pulse radiographic system," in *Proc. IEEE 21st Int. Conf. Pulsed Power (PPC)*, Brighton, U.K., Jun. 2017, pp. 1–6.

[19] T. P. Hughes, C. B. Mostrom, T. C. Genoni, and C. Thoma, "LAMDA user's manual and reference," Voss, Norway, Vestland, Tech. Rep. VSL-0707, 2007.

[20] P. Allison *et al.*, "Beam-breakup calculations for the DARHT accelerator," in *Proc. 14th Particle Accel. Conf.*, San Francisco, CA, USA, 1991, p. 520.

[21] C. Ekdahl, "Cathode to target simulations for scorpius: I. Simulation codes and models," 2021, *arXiv:2104.14593*.

[22] C. Ekdahl and R. McCrady, "BBU suppression by stagger tuning," Los Alamos Nat. Lab., Santa Fe, NM, USA, Tech. Rep. LA-UR-20-20781, 2020.

[23] R. McCrady, "Transverse impedance," Los Alamos Nat. Lab., Santa Fe, NM, USA, Tech. Rep. LA-UR-19-25391, 2019.

[24] G. J. Caporaso *et al.*, "Beam dynamics in the advanced test accelerator (ATA)," in *Proc. 5th Int. Conf. High Power Partticle Beams*, San Francisco, CA, USA, 1983, pp. 427–433.

[25] E. G. Cook *et al.*, "Inductive-adder kicker modulator for DARHT-2," in *Proc. Int. Linac Conf.*, Monterey, CA, USA, 2000, pp. 1–5.

[26] E. J. Gower and J. S. Sullivan, "Analog amplitude modulation f a high voltage solid state inductive adder pulse generator using MOSFETs," in *Proc. Int. Power Modulator Conf.*, Hollywood, CA, USA, 2002, pp. 321–324.

[27] E. G. Cook *et al.*, "Solid-state modulators for RF and fast kickers," in *Proc. Part. Accel. Conf.*, Knoxville, TN, USA, 2005, pp. 637–641.

[28] C. Ekdahl, "Beam envelope stability in an advanced linear induction accelerator," *IEEE Trans. Plasma Sci.*, vol. 49, no. 10, pp. 3092–3098, Oct. 2021.

[29] M. Burns *et al.*, "Cell design for the DARHT linear induction accelerators," in *Proc. Conf. Rec. IEEE Part. Accel. Conf.*, San Francisco, CA, USA, 1991, pp. 1–6.

[30] *CST Studio Suite*. Accessed: Feb. 4, 2022. [Online]. Available: https://www.3ds.com/products-services/simulia/products/cst-studio-suite/

[31] S. S. Kurennoy and R. C. McCrady, "Beam coupling impedances of ferrite-loaded cavities: Calculations and measurements," in *Proc. Int. Part. Accel. Conf.*, Campinas, Brazil, 2021, pp. 696–699.

[32] S. A. Heifets and S. A. Kheifets, "Coupling impedance in modern accelerators," *Rev. Mod. Phys.*, vol. 63, pp. 631–673, Oct. 1991.

[33] R. J. Briggs and W. Fawley, "Campaign to minimize the transverse impedance of the DARHT-2 induction linac cells," Lawence Berkeley Nat. Lab., Berkeley, CA, USA, Tech. Rep. LBNL-56796(Rev-1), 2002.

[34] Y. Tang, T. P. Hughes, C. A. Ekdahl, and K. C. D. Chan, "BBU calculations for beam stability experiments on DARHT-2," in *Proc. Eur. Part. Accel. Conf.*, Edinburgh, Scotland, 2006, pp. 1–23.